PrimPol-dependent single-stranded gap formation mediates homologous recombination at bulky DNA adducts

Ann Liza Piberger[1], Alexandra K Walker[1], Joanna R Morris[1], Helen E Bryant[2], Eva Petermann[1,*]

[1]Institute of Cancer and Genomic Sciences, College of Medical and Dental Sciences, University of Birmingham, Birmingham B15 2TT, United Kingdom

[2]Department of Oncology & Metabolism, The Medical School, University of Sheffield, Sheffield S10 2RX, United Kingdom

*Corresponding authors: A.L.Piberger@bham.ac.uk; E.Petermann@bham.ac.uk

Running title: Re-priming-mediated recombination

Summary

Obstacles on the DNA template can lead to DNA replication fork stalling and genomic rearrangements. RAD51-mediated homologous recombination (HR) can promote restart and repair of stalled forks, but also post-replicative repair once the obstacle has been bypassed. Bulky DNA adducts are important replication-blocking lesions induced by environmental carcinogens, but it is not known whether they activate HR directly at stalled forks, or at gaps left behind ongoing forks. Here we show that in mammalian cells, bulky adducts predominantly induce HR at post-replicative gaps formed by the DNA/RNA primase PrimPol. Using BPDE and UV model lesions, we report that RAD51 is not recruited to stalled or collapsed forks, but instead to long gaps formed by PrimPol re-priming activity and resection by MRE11 and EXO1. In contrast, RAD51 loading at DSBs does not require PrimPol. At bulky adducts, PrimPol is required for the induction of sister chromatid exchanges and genetic recombination. Our data support that HR at bulky adducts in mammalian cells is primarily associated with post-replicative gap repair and define a role for PrimPol in DNA damage tolerance by homologous recombination.

Introduction

A proper cell response to DNA damage during DNA replication is essential to maintain genome integrity and prevent cancer development. Environmental exposures frequently induce bulky DNA adducts, mutagenic and carcinogenic DNA lesions that can pose strong physical obstacles to DNA replication forks. If not removed by nucleotide excision repair (NER), then the presence of these adducts on the DNA template inhibits the replicative polymerase, potentially leading to replication fork stalling. If stalled forks cannot be restarted, they can collapse into DNA double strand breaks (DSBs), which are highly toxic and/or mutagenic. Fork collapse also activates homologous recombination (HR) for repair (Arnaudeau et al., 2001; Saintigny et al., 2001).

HR proteins, such as RAD51, are also involved in the remodelling and restart of stalled forks. We previously showed that replication inhibitors such as hydroxyurea induce at least two different RAD51-mediated HR pathways.

Stalled forks recruit small amounts of RAD51 for restart, while HR repair of forks that have been collapsed into double strand breaks (DSBs) requires more extensive RAD51 loading and formation of RAD51 foci (Petermann et al., 2010). RAD51 functions at stalled forks have since then been linked to replication fork reversal (Zellweger et al., 2015), fork protection by preventing MRE11 resection (Schlacher et al., 2011), and promoting continuous replication through interaction with DNA Pol alpha (Kolinjivadi et al., 2017). Sources of bulky adducts, such as UV radiation or the environmental mutagen benzo[*a*]pyrene-diol-epoxide (BPDE), strongly induce RAD51 foci formation and HR, suggesting that these lesions stall and collapse forks. However, bulky DNA lesions can also be bypassed using DNA damage tolerance pathways, which avoid fork stalling. Damage tolerance can occur through re-priming, for example by PrimPol (Bianchi et al., 2013; Elvers et al., 2011; Mourón et al., 2013), error-prone translesion synthesis (TLS) that is promoted by PCNA mono-ubiquitination, or an error free damage tolerance pathway that is promoted by PCNA polyubiquitination and also uses recombination proteins.

This last pathway requires RAD51 and involves template switching to the undamaged sister chromatid. Mechanistically, template switching is still poorly understood. It has been proposed to operate either directly at the stalled fork, using fork reversal, or at post-replicative gaps behind the fork, while the fork itself continues by re-priming (Branzei and Szakal, 2017). In budding yeast, there is evidence that re-priming and post-replicative gap filling is preferred over fork reversal, and this pathway has been shown to involve a double Holliday junction-like intermediate (Fumasoni et al., 2015; Giannattasio et al., 2014). Although it has been proposed since the 1970s that re-priming at DNA lesions can also lead to recombination in mammalian cells, fork reversal has been reported to be frequent in mammalian backgrounds (Zellweger et al., 2015), and may be preferred over re-priming.

Therefore, a longstanding and important mechanistic question is: where is RAD51 most important for replication bypass of bulky lesions, at the fork or behind the fork? Does the observed HR activity at bulky lesions occur at stalled forks, collapsed forks or post-replicative gaps, and what are the molecular mechanisms involved?

To address these questions, we used BPDE and UV lesions as models to investigate HR induction at bulky DNA adducts in human cells. Like UV lesions, BPDE adducts are highly relevant to human disease. They are induced by the common environmental carcinogen benzo[a]pyrene (B[a]P). B[a]P is one of the most potent known carcinogens and ubiquitous in emissions from traffic, industry, stoves and cigarette smoke (Choi et al., 2010; IARC, 2012). BPDE adducts cause the specific mutation signature of smoking-induced lung cancer (Alexandrov et al., 2016; Kucab et al., 2019). They are weak substrates for NER, and unrepaired adducts are ubiquitously detectable in the DNA of individuals(Geacintov and Broyde, 2017; Villalta et al., 2017). BPDE adducts can be bypassed in both error-free and error-prone manner by TLS polymerases (Livneh et al., 2010; Rechkoblit et al., 2017). However, and in contrast to UV-induced cyclobutane pyrimidine dimers (CPDs), when replication encounters lower and more physiologically relevant levels of BPDE adducts, this predominantly induces HR (Cohen et al., 2015; Izhar et al., 2013). BPDE adducts are thus highly recombinogenic and excellent model lesions for studying HR at bulky adducts (Fig. 1A).

Using low concentrations of BPDE that are non-toxic and recombinogenic, we report that RAD51 foci formation and HR activation in response to bulky DNA adducts does not result from replication fork stalling or -collapse. Instead, RAD51 is recruited onto post-replicative single-stranded gaps that are generated by the re-priming activity of PrimPol and extensively resected. Our data support that HR activity at bulky adducts in mammalian cells is predominantly associated with post-replicative repair, and define a role for PrimPol in DNA damage tolerance.

Results

RAD51 foci form at bulky DNA adducts in absence of fork stalling or -collapse

To investigate HR at bulky DNA adducts, U2OS cells were treated with BDPE for 20 min followed by release into fresh medium. After this treatment, BPDE lesions persist for more than 24 hours due to slow repair (Piberger et al.,

2018). We chose a range of concentrations from low non-toxic (50 nM) to high and cytotoxic doses (500 nM and 1.65 µM) (Figure S1A). BPDE induced phospho-S139 histone H2AX (γH2AX) foci that co-localised with 5-Chlorodeoxyuridine (CldU) foci marking ongoing replication forks, supporting that the treatment was causing replication stress (Fig. 1B). γH2AX foci were induced equally across all BPDE concentrations and persisted for at least 24 hours, in line with inefficient repair (Fig. 1C). RAD51 foci analysis showed that HR was induced over several days after release from BPDE. In agreement with previous studies(Cohen et al., 2015; Izhar et al., 2013), the percentage of RAD51 foci positive cells was more strongly increased after release from 50 nM BPDE compared to higher BPDE doses (Fig. 1D, E). This was not due to cell cycle changes as 50 nM BPDE had minimal effects on cell cycle distribution (Fig. S3A). Furthermore, the numbers of RAD51 foci per foci positive cell were also strongly increased after 50 nM BPDE (Fig S1B).

We next determined the impact of BPDE treatment on replication fork slowing and -stalling. This first required developing optimised CldU and IdU dual pulse-labelling protocols for DNA fibre analysis. We initially added BPDE with the second (IdU) label to measure the immediate effect of BPDE on replication fork progression. Only very high BPDE concentrations (1.65 µM) strongly slowed replication speeds (Fig. S1C). To measure replication fork stalling, we labelled U2OS cells with CldU before, during and for 30 min after the BPDE incubation to detect forks that stalled either during or after the treatment. Cells were then washed and labelled with IdU to detect any ongoing forks for a further 20 min (Fig. 1F). Surprisingly, we found that while higher BPDE concentrations increased fork stalling, 50 nM BPDE did not lead to appreciable increase in stalled forks (Fig. 1F).

Analysis of 53BP1 foci, a DSB marker, suggested that 50 nM BPDE induced far fewer DSBs compared to higher BPDE doses (Fig. 1G). This was further confirmed by physical detection of DSBs using pulse-field gel electrophoresis (Fig. S1D, E). These data suggested that RAD51 foci induced by 50 nM BPDE were not connected with DSB formation. In contrast, RAD51 foci induced by higher BPDE concentrations correlated well with DSB formation

(Fig. 1E, G). This posed the question as to the mechanism and role of RAD51 foci formation specifically after low dose BPDE treatment.

Surprisingly, siRNA depletion of RAD51 did not have a large impact on levels of stalled forks after release from low (50 nM) or high (1.65 µM) BPDE concentrations (Fig. 1H, I, Fig. S1F). This suggested that RAD51 was not required to promote fork restart under these conditions. RAD51 can also promote fork slowing or -stalling at lesions induced by UV or MMS (Ronson et al., 2018; Vallerga et al., 2015). However, we found no evidence that RAD51 promoted fork slowing on BPDE-damaged templates (Fig. S1G). Further, RAD51 is required for the repair of collapsed forks and prevents DSB accumulation in response to hydroxyurea (Petermann et al., 2010). However, RAD51 depletion had no major effect on the levels of 53BP1 foci induced by either 50 nM or 500 nM BPDE (Fig. 1J, Fig. S1H). These data suggested that RAD51 is also not involved in preventing fork collapse or repairing collapsed forks in response to BPDE lesions.

PrimPol-dependent re-priming promotes ssDNA gap formation at bulky DNA adducts

RAD51 loading to initiate HR requires formation of long stretches of ssDNA that are initially coated with RPA, which is then exchanged for RAD51. RPA foci analysis showed that ssDNA was rapidly formed even after release from 50 nM BPDE, in absence of fork stalling or DSB formation (Fig. S2A, B). RAD51 depletion impaired the resolution of these RPA foci after release from BPDE, suggesting that RAD51 was involved in resolution of BPDE-induced ssDNA (Fig. 2A).

To specifically test whether ssDNA gaps were formed at BPDE lesions behind ongoing forks, we used the S1 endonuclease (S1)-modified fibre assay (Quinet et al., 2017). S1-dependent DNA cleavage of ssDNA gaps or nicks allows to specifically detect these lesions in newly replicated DNA (Fig. 2B). After DNA fibre labelling, nuclei are permeabilised and treated with recombinant S1 nuclease before DNA fibre spreading and staining. If ssDNA gaps are present in nascent DNA, the S1-induced DSBs cause shortening of

the IdU-labelled fibres, thereby increasing CldU/IdU ratios. S1 nuclease treatment after fibre labelling with 50 nM BPDE for 20 min resulted in an increased CldU/IdU ratio compared to all other conditions, supporting that ssDNA gaps were generated during replication of DNA containing BPDE lesions (Fig. 2C).

Taken together, these data suggested that RAD51 is involved in post-replicative repair and that the RAD51 foci nucleation site might be at regions of ssDNA away from the ongoing fork. We hypothesised this ssDNA might form at post-replicative gaps through re-priming of DNA synthesis downstream of the bulky lesion (Fig. 2D).

We therefore investigated a potential role for re-priming in ssDNA gap formation. The RNA/DNA primase PrimPol was recently reported to re-prime after UV lesions (Bianchi et al., 2013; Garcia-Gomez et al., 2013; Mourón et al., 2013) and was therefore a good candidate for promoting ssDNA gap formation (Fig. 2D). We used siRNA to deplete PrimPol in U2OS cells. Due to the difficulty in detection of PrimPol with antibodies, qRT-PCR was used to confirm depletion (Fig. 2E). We first tested whether PrimPol re-priming was responsible for the continued fork progression and lack of fork stalling after treatment with 50 nM BPDE. Indeed, we observed that 50 nM BPDE induced fork stalling specifically when PrimPol was depleted (Fig. 2F). Furthermore, PrimPol depletion prevented ssDNA gap induction as measured by S1 nuclease fibre assay (Fig. 2G). PrimPol exerts both DNA/RNA primase and DNA polymerase activity (Guilliam and Doherty, 2017). To test whether the PrimPol primase activity is specifically required for continued replication fork progression in presence of BPDE, we performed rescue experiments in PrimPol-depleted cells by ectopically expressing wild type (WT) and primase-dead (CH) mutant versions of PrimPol (Martinez-Jimenez et al., 2018; Mourón et al., 2013) (Fig. 2H, I, J). Only WT PrimPol, but not CH PrimPol, could rescue BPDE-induced fork stalling, supporting that re-priming prevents BPDE-induced fork stalling (Fig. 2J, Fig. S2C).

PrimPol-mediated re-priming and further end processing promote RAD51 loading

We next investigated whether RAD51 foci formation itself depended on PrimPol-mediated re-priming and ssDNA gap formation. PrimPol depletion strongly reduced RAD51 foci formation after treatment with 50 nM BPDE (Fig. 3A, B). This was not due to changes in the S/G2 phase population, as PrimPol- and control-depleted cells displayed similar cell cycle profiles with and without BPDE treatment (Fig. S3A). RAD51 foci formation in PrimPol-depleted cells could be rescued by ectopic expression of PrimPol WT, but not the primase-dead PrimPol CH mutant, again suggesting that specifically the re-priming activity is required for RAD51 foci formation (Fig. 3C).

In vitro experiments suggest that PrimPol re-primes around 14 nucleotides downstream of DNA lesions (Kobayashi et al., 2016). Such short ssDNA gaps would need further resection by nucleases such as MRE11 and Exonuclease 1 (EXO1) to allow for RAD51 foci formation (Fig. 3D). To investigate the lengths of these gaps, we used Single Molecule Analysis of Resection Tracks (SMART) (Cruz-Garcia et al., 2014). Cells were treated with BrdU for 48 hours to BrdU-label all DNA. DNA fibre spreading followed by BrdU immunostaining without acid denaturation was then used to visualise stretches of ssDNA. While there were no detectable ssDNA stretches in control samples, BPDE treatment induced long tracks of single-stranded DNA (5 – 30 kb) (Fig. 3E, F). To investigate the contribution of resection activities, we used PFM01, a chemical inhibitor of the endonuclease activity of MRE11. PFM01 treatment reduced the lengths of the ssDNA tracks (Fig. 3E, F) although it did not entirely suppress ssDNA track formation. This suggested that either the exonuclease activity of MRE11 or other resection factors were also involved in ssDNA track formation. We then investigated the impact of resection on RAD51 foci formation, using chemical inhibitors of the exo- and endonuclease activities of MRE11 (mirin and PFM01, respectively) as well as siRNA depletion of EXO1. MRE11 activity and EXO1 were both required for BPDE-induced RAD51 foci formation, supporting that PrimPol-mediated HR initiation involves resection (Fig 3G, H).

PrimPol re-priming promotes RAD51 loading at bulky DNA adducts, but not in response to DSB-inducing conditions

To investigate the relevance of PrimPol re-priming for HR initiation at other bulky lesions, we used UV-C irradiation to induce CPD and 6-4 photoproducts and measured the impact on ssDNA gap formation in presence and absence of PrimPol (Fig 4A). UV-C irradiation induced large amounts of S1 endonuclease-sensitive sites, but this was largely abrogated after PrimPol depletion (Fig. 4B). Furthermore, PrimPol was required for efficient RAD51 foci formation in response to bulky lesions induced by UV-C, although the effect was overall smaller than at BPDE lesions (Fig. 4C). This is probably because UV-induced recombination has been shown to also be partly dependent on NER (Ma et al., 2013). Taken together, these data suggest that PrimPol-mediated re-priming generates ssDNA gaps for RAD51 loading at bulky DNA adducts more widely.

We then investigated whether PrimPol is required for RAD51 foci formation in response to other types of DNA damage. After treatment with 500 nM BPDE, which induces only DSB-associated HR after fork stalling (Fig. 1E-G), PrimPol was not required for RAD51 loading (Fig. 4D). PrimPol re-priming still occurred at 500 nM BPDE (Fig. S3B, C), but the observation that re-priming does not promote RAD51 loading at this concentration is consistent with published data that high BPDE damage loads favour TLS over HR (Cohen et al., 2015; Izhar et al., 2013).

PrimPol was also not required for RAD51 loading in response to 24 hours HU or in response to ionising radiation (IR), which both induce DSB (Petermann et al., 2010) (Fig. 4E, F). The lack of a role for PrimPol in DSB-induced recombination agrees with the standard model of RAD51 loading onto resected DSB ends, which does not require any re-priming.

PrimPol-mediated ssDNA gap formation promotes homologous recombination and sister chromatid exchange

Finally, we investigated whether PrimPol-mediated re-priming is required to support activation of the complete HR pathway leading to genetic recombination. We analysed BPDE-induced HR frequencies using the reporter cell line SW480SN.3, which harbours the SCneo recombination reporter construct that can detect HR by unequal sister chromatid exchange, intrachromatid exchange, single-strand annealing or gene conversion (Johnson et al., 1999). 50 nM BPDE induced measurable HR in this reporter, and this was reduced after PrimPol depletion (Fig 5A, Fig. S4A). In contrast, PrimPol depletion had no effect on colony survival or percentage of sub-G1 population after BPDE treatment, and the impact of RAD51 depletion on survival was also very small (Fig 5B, Fig. S4B). PrimPol depletion did also not increase DSB formation after BPDE treatment (Fig. S4C). This is in line with previous findings that PrimPol-depleted human cells are not very UV-sensitive, suggesting that TLS or other pathways can compensate (Bianchi et al., 2013). It also suggests that the PrimPol-mediated pathway might predominantly impact on BPDE-induced mutagenesis and/or the level of genomic rearrangement found in cells. 50 nM BPDE induced genomic rearrangements in the form of sister chromatid exchanges (SCEs) (Fig 5C, D). SCE formation is usually attributed to collapsed fork repair, but according to some models, SCEs could also arise from post-replicative template switching (Dong and Fasullo, 2003). PrimPol depletion prevented BPDE-induced SCE formation, while it did not influence the amount of SCEs under undamaged conditions (Fig. 5E).

Discussion

We have shown that during DNA replication of bulky DNA adducts in mammalian cells, HR activation does not occur at stalled or collapsed replication forks but instead at single-stranded gaps that are generated by the re-priming activity of PrimPol (Fig. 5F). This pathway that has both similarities and differences to DSB repair.

Previous work has suggested roles for re-priming and PrimPol at UV lesions (Bianchi et al., 2013; Elvers et al., 2011; Garcia-Gomez et al., 2013; Mourón et al., 2013). It is therefore not very surprising that re-priming also occurs at other bulky lesions. However, our findings address long-standing questions by showing that at bulky DNA adducts, RAD51 foci formation and sister chromatid exchange that have been traditionally connected with replication fork collapse and DSB repair, are instead associated with the repair of post-replicative gaps. Furthermore, these gaps are produced by PrimPol, shedding light on the function of PrimPol during DNA damage tolerance.

Why are these post-replicative gaps resected and channelled into HR rather than simply filled by TLS? We speculate that HR and TLS-dependent gap filling could compete at ssDNA gaps. Gap resection might prevent TLS and promote HR, but TLS might be preferred over resection under high damage load. It will be important to decipher whether and how PrimPol re-priming and the presence of the bulky adduct influence the pathway decision between TLS and template switching.

Our data agree with recent work in budding yeast, reporting that checkpoint activation by fork-stalling lesions also occurs at EXO1-resected post-replicative gaps rather than directly at the fork (Garcia-Rodriguez et al., 2018a). Furthermore, EXO1 resection is downstream of PCNA polyubiquitylation that promotes template switching. A model was proposed in which resection of the gap is stimulated by polyubiquitylated PCNA stuck on the 3' (upstream) junction and by the 9-1-1 checkpoint clamp loaded onto the 5' (downstream) junction (Garcia-Rodriguez et al., 2018b) (Fig. 5F). However the gaps that have been observed after UV treatment in budding yeast and *X. laevis* egg extracts are less than 1 kb long (Hashimoto et al., 2010; Lopes et al., 2006). Our data suggest BPDE-induced gaps are much longer, similar to the extent of resection at DSBs, or gaps induced by HU in budding yeast (Gallo et al., 2019; Zhou et al., 2014). The length of these gaps could result from PrimPol actually re-priming far away from the lesion, and/or from long-range resection.

With the observed roles for resection and RAD51 foci formation, HR at bulky adducts seems to resemble DSB repair more than the known HR functions at

stalled forks. It has been speculated pro-recombination activities could be specifically recruited to the post-replicative environment at the gap (Branzei and Szakal, 2017). These may promote RAD51 foci formation, and long-range resection may support more accurate homology search. In contrast at stalled replication forks, RAD51 foci formation might be suppressed by anti-recombinogenic helicase activities (Branzei and Szakal, 2017) and the possibilities for remodelling, e.g. by fork reversal (Fig. 5F).

Another unanswered question is the contribution of re-priming by DNA polymerase α (Pol α) to HR. Pol α is solely responsible for gap formation in yeast, which lack PrimPol (Fumasoni et al., 2015). In mammalian cells, with Pol α constantly re-re-priming on the lagging strand and possibly also the leading strand, one would expect at most half of gap- and RAD51 foci formation to be PrimPol-dependent. Recent work has suggested that in budding yeast, different pathways act on the leading and lagging strands (Rosenbaum et al., 2019) it will be interesting to investigate whether only re-priming via PrimPol promotes HR-dependent gap repair, possibly due to PrimPol's preference to synthesise DNA primers.

While we have shown that PrimPol re-priming initiates HR at UV and BPDE DNA adducts, we speculate that other bulky lesions or replication impediments can be channelled into this pathway. DNA-protein crosslinks for example engage HR for repair (Fang, 2013; Nakano et al., 2007) and lead to template-switching (Laranjo et al., 2018) raising the question whether PrimPol acts at these lesions as well. PrimPol also re-primes at R-loops and secondary structure-forming sequences (Svikovic et al., 2018) , opening up the possibility that HR in those backgrounds might depend at least partially on PrimPol. It will be important to test how commonly PrimPol promotes recombination at other DNA lesions.

Understanding the molecular mechanism of HR induced by bulky adducts is important for human health. We suggest that this will be particularly useful to interpret more recent cancer genomics data. Both BPDE-treated cells and lung cancers harbour insertion and deletion mutations (indels) of unknown origin. These are in addition to the point mutations ascribed to error-prone TLS (Alexandrov et al., 2016; Schiltz et al., 1999). Indels could result from

replication-associated HR, such as at restarting forks (Carr and Lambert, 2013), or from defective HR, such as in BRCA-mutant cancers (Zamborszky et al., 2017). It is therefore important to decipher which HR pathways are actually induced by bulky adducts. Furthermore, genetic variants in the HR genes *BRCA2* and *RAD52* have been liked to lung cancer susceptibility (Lieberman et al., 2016; Wang et al., 2014). It will be important to investigate the impact of such genetic variants on HR at ssDNA gaps. A *PRIMPOL* variant has also been suggested to play a potential role in cancer (Diaz-Talavera et al., 2019).

Taken together, our data support that a large fraction of mammalian replication-associated HR occurs after re-priming, post-replicatively behind the fork.

Materials and Methods

Cell lines and reagents

U2OS and A549 cells were obtained from ATCC. The SW480SN.3 cell line has been described before (Saleh-Gohari et al., 2005). Cells were confirmed to be free of Mycoplasma infection and grown in Dulbecco's modified Eagle's Medium (DMEM) with 10% foetal bovine serum in a humidified atmosphere containing 5% CO_2. Media was additionally supplemented with L-Glutamine (2 mM), Penicillin (50 U/mL), and Streptomycin (50 µg/mL). Additionally, SW480SN.3 cells were grown in hygromycin (50 µM) to maintain the SCneo recombination reporter.

(+)-*anti*-B[a]P-7*R*,8S-dihydrodiol-9*S*,10*R*-epoxide (enantiopure, BPDE) was custom-synthesised by the Biochemical Institute for Environmental Carcinogens (Grosshansdorf, Germany). Mirin, PFM01 and hydroxyurea (HU) were from Sigma-Aldrich.

Immunofluorescence

Cells were fixed with 4% PFA for 10 min and permeabilised with 0.25% triton X-100 for 5 min at 4°C followed by blocking with 4% FCS in PBS. Primary antibodies were rabbit polyclonal anti-RAD51 (Abcam ab63801, 1:800 or Calbiochem PC130, 1:2,000 for IR-induced RAD51 foci), mouse monoclonal

anti-phospho-Histone H2AX (Ser139) (JBW301, Millipore, 1:1,000), rabbit polyclonal anti-53BP1 (Bethyl A300-272A, 1:15,000), mouse anti-RPA32 (Merck NA18, 1:500), mouse monoclonal anti-BrdU (B44, Becton Dickinson 347580, 1:50) to detect CldU. Secondary antibodies were anti-rabbit IgG AlexaFluor 555 and anti-mouse IgG AlexaFluor 488 (ThermoFisher). For RPA staining, cells were pre-extracted with CSK buffers (CSK1: 10 mM PIPES, 300 mM sucrose, 100 mM NaCl, 3 mM $MgCl_2$, CSK2: 0.5 % triton X) on ice previous to PFA fixation. For RAD51 foci detection in response to IR irradiation, cells were also pre-extracted and subjected to EdU staining to label replicating cells. To this end, cells were incubated with EdU at a final concentration of 1 µM for 30 min before staining was carried out as detailed in Click-iT EdU Imaging Kits (Life Technologies). For co-localisation staining, primary and secondary antibodies against phospho-Histone H2AX were fixed for 10 min with 2% PFA before DNA denaturation with 2M HCl for 40 min and immunostaining for CldU. DNA was counterstained with DAPI. Cells with more than 5 RAD51 foci (10 foci for IR-induced RAD51 staining) and 8 γH2AX or 10 53BP1 foci were scored as positive.

DNA fibre analysis

U2OS cells were pulse labelled with 25 µM CldU and 250 µM IdU, and treated with BPDE for the times indicated. Labelled cells were harvested and DNA fibre spreads were incubated with rat anti-BrdU (BU1/75, Abcam ab6326, 1:700) and mouse anti-BrdU (B44, Becton Dickinson 347580, 1:500) for 1 h, fixed with 4% PFA and incubated with anti-rat AlexaFluor 594 and anti-mouse AlexaFluor 488 (Thermo Fisher) for 1.5 h. Fibers were examined using a Nikon E600 microscope with a Nikon Plan Apo 60x (1.3 NA) oil lens, a Hamamatsu digital camera (C4742-95) and the Volocity acquisition software (Perkin Elmer). For quantification of replication structures, at least 190 structures were counted per experiment. For quantification of fork speeds, the lengths of labelled tracks were measured using the ImageJ software (http://rsbweb.nih.gov/ij/) (Schneider et al., 2012) and arbitrary length values were converted into µm using a micrometer slide for calibration.

S1 endonuclease (S1)-modified DNA fibre assay

The S1-modified DNA fibre assay was carried out as described before (Quinet et al., 2017) . Briefly, U2OS cells were pulse labelled with 25 μM CldU and 250 μM IdU, and treated with BPDE for the times indicated followed by permeabilization with CSK100 buffer (100 mM NaCl, 10 mM MOPS pH 7.0, 3 mM $MgCl_2$, 300 mM sucrose, 0.5% triton X-100) for 10 min. Nuclei were subsequently treated with either 20 U/mL S1 endonuclease (Invitrogen Cat # 18001016) to induce DSBs at sites of DNA gaps or mock-treated (S1 buffer: 30 mM sodium acetate, 10 mM zinc acetate, 5% glycerol, 50 mM NaCl, pH 4.6) for 30 min at 37°C. Nuclei were harvested by scraping and DNA fibre spreads were prepared and stained and analysed as described for the unmodified fibres assay above. At least 120 fibres per condition were measures from 3 independent biological repeats.

Single Molecule Analysis of Resection Tracks (SMART)

SMART assay was performed as described (Densham et al., 2016). U2OS cells were treated with 20 μM BrdU for 48 h. After treatment with BPDE and MRE11 inhibitor, DNA was spread as for the unmodified DNA fibre assay. Native fibre spreads were stained with mouse anti-BrdU (B44, Becton Dickinson 347580, 1:500) for 1 h, fixed with 4% PFA and incubated with anti-mouse AlexaFluor 488 (Thermo Fisher) for 1.5 h. Fibers were examined as described above. For quantification of DNA gap sizes, the lengths of green (AF 488) labelled native patches were measured using ImageJ and arbitrary length values were converted into μm using the scale bars created by the microscope. A total of at least 550 fibre stretches derived from 3 independent biological repeats were measured.

Pulsed-field gel electrophoresis (PFGE)

DSBs were detected via PFGE as described before (Jones et al., 2014) . Briefly, $2x10^6$ cells per sample were treated as indicated, harvested and melted into 1.0% InCert-Agarose (Lonza) inserts. Inserts were digested in 0.5 M EDTA-1% *N*-laurylsarcosyl-proteinase K (1 mg/ml) at room temperature for 48 h and washed three times in TE buffer. Inserts were loaded onto a separation gel (1.0% chromosomal-grade agarose, Bio-Rad). Separation was

performed using a CHEF DR III (BioRad; 120 field angle, 240 s switch time, 4 V cm^{-1}, 14 °C) for 20 h. Images of ethidium bromide-stained gels were acquired using a Syngene G:BOX gel imaging system. DSBs (chromosome fragments >2 Mbp) were quantified by densitometry using ImageJ and normalized to the total amount of DNA in the gel.

siRNA and DNA transfection

Custom made siRNAs against RAD51 (Ito et al., 2005) , and PrimPol (Bianchi et al., 2013) were from Dharmacon, and custom made EXO1 siRNA (Sense: GAA CAA GGU UCC UGG GCU AUA[dT][dT], Antisense: [Phos]UAU AGC CCA GGA ACC UUG UUC[dT][dT]) was from Sigma-Aldrich. “Allstars negative control siRNA” was from Qiagen. Cells were transfected for 48 h with 50 nM siRNA using Dharmafect 1 reagent (Dharmacon). For combined siRNA and PrimPol expression, cells were transfected for 48 h using TransIT-X2 (Mirus Bio) with 50 nM siRNA and 1.5 µg PrimPol variant expressing pcDNA/V5-tag vectors (Mourón et al., 2013) or control plasmid pEGFP-C2 (Clontech).

Western blotting

Cell extracts were prepared in UTB buffer (50 mM Tris-HCl pH 7.5, 150 mM β-mercaptoethanol, 8 M urea) and sonicated to release DNA-bound proteins. Primary antibodies used were rabbit anti-RAD51 (Abcam, ab63801, 1:1,000), rabbit anti-EXO1 (Bethyl, A302-640, 1:1,000), mouse anti-V5 tag (Invitrogen, R960-25, 1:1:500), mouse anti-αTUBULIN (B512, Sigma T6074, 1:10,000), mouse anti-PARP1 (Santa Cruz, sc-8007, 1:500).

Quantitative RT-PCR

Total RNA was harvested using the miRNeasy Mini Kit (Qiagen) followed by DNase I treatment (Roche). 1 µg of total RNA was reverse-transcribed using SuperScript Reverse Transcriptase III (Thermo Fisher) with random primers (Promega), following manufacturer’s instructions. The qPCR primers for amplification are listed in Table S1. For quantitative RT-PCR, 2 µl of cDNA were analyzed using a CFX Connect real-time PCR machine (BioRad) with SensiFAST SYBR Lo-ROX Kit (Bioline). Cycling parameters were 95°C for 3 min, followed by 40 cycles of 95°C for 10 s, 60°C for 30 s. Result were

normalised to RPLP0. ΔcT was calculated as difference in the cycle threshold of the transcript of interest and RPLP0, plotted as fold change compared to the CTR untreated sample.

Recombination in SW480SN.3 cells

Following siRNA treatments, SW480SN.3 cells were rinsed in PBS and left in fresh non-selective media for 48 h. Cells were treated with solvent or 50 nM BPDE for 20 min, rinsed in 2x PBS, trypsinized and directly reseeded. To determine cloning efficiency, two dishes were plated with 500 cells each. For selection of recombinants cells were grown in G418 (1 mg/ml; 25 cells/mm^2) in two technical repeats. After 14-18 days the colonies obtained were stained with methylene blue in methanol (4 g/l) and the number of recombinants was calculated per 10^{-5} colony forming cells.

Analysis of sister chromatid exchange (SCE)

U2OS were incubated with 240 µM BrdU for two cell cycles and treated with BPDE or siRNA as indicated, and SCE analysis was performed as described (Hoh et al., 2011). SCEs were defined by an exchange of dark-stained (Hoechst-bound TT-rich) segments with light, bleached (BrdU incorporated) segments. Staining variation where chromatids clearly twisted around each other was excluded from the count. For each condition, at least 90 metaphases from at least 3 independent biological repeats were analysed. SCE rates were calculated per diploid set of chromosomes to compensate although U2OS present with chromosome counts in the hypertriploid range.

Colony survival assay

U2OS cells were siRNA transfected for 24 h previous to being plated in triplicates for both 500 and 1,000 cells. Cells were given 24 h to adhere before treatment with BPDE (10 – 400 nM) for 20 min. Subsequently, cells were washed 2 x PBS and colonies of >50 cells were allowed to form in fresh medium and fixed in 50% ethanol, 2% methylene blue.

Flow cytometry

U2OS cells were transfected with siRNA for 48 h followed by treatment with 50 nM BPDE and release into fresh DMEM. After the indicated release times,

cells were fixed with ice-cold 70% ethanol before staining with 50 µg/ml propidium iodide and 100 µg/ml RNase H solution overnight. Cell cycle profiles were gathered using the BD LSR Fortessa X20 and analysed with BD FacsDiva software.

Quantification and statistical analysis

Values represent the means + 1x SEM of at least 3 independent biological repeats. For foci analysis, at least 10 different areas were quantified for each independent biological repeat. The number of independent biological repeats (n) is indicated in the figure legends. The statistical test used throughout was the one-tailed student's t-test. Asterisks compare to control, unless indicated otherwise in the figure panels, and signify *p<0.05, **p<0.01, ***p<0.001.

References

Alexandrov, L.B., Ju, Y.S., Haase, K., Van Loo, P., Martincorena, I., Nik-Zainal, S., Totoki, Y., Fujimoto, A., Nakagawa, H., Shibata, T.*, et al.* (2016). Mutational signatures associated with tobacco smoking in human cancer. Science *354*, 618-622.

Arnaudeau, C., Lundin, C., and Helleday, T. (2001). DNA double-strand breaks associated with replication forks are predominantly repaired by homologous recombination involving an exchange mechanism in mammalian cells. J Mol Biol *307*, 1235-1245.

Bianchi, J., Rudd, S.G., Jozwiakowski, S.K., Bailey, L.J., Soura, V., Taylor, E., Stevanovic, I., Green, A.J., Stracker, T.H., Lindsay, H.D.*, et al.* (2013). PrimPol bypasses UV photoproducts during eukaryotic chromosomal DNA replication. Mol Cell *52*, 566-573.

Branzei, D., and Szakal, B. (2017). Building up and breaking down: mechanisms controlling recombination during replication. Critical reviews in biochemistry and molecular biology *52*, 381-394.

Carr, A.M., and Lambert, S. (2013). Replication stress-induced genome instability: the dark side of replication maintenance by homologous recombination. J Mol Biol *425*, 4733-4744.

Choi, H., Komulainen, H., and Delgado Saborit, J.M. (2010). WHO guidelines for indoor air quality: selected pollutants. (WHO Regional Office for Europe), pp. 289-346.

Cohen, I.S., Bar, C., Paz-Elizur, T., Ainbinder, E., Leopold, K., de Wind, N., Geacintov, N., and Livneh, Z. (2015). DNA lesion identity drives choice of

damage tolerance pathway in murine cell chromosomes. Nucleic Acids Research *43*, 1637-1645.

Cruz-Garcia, A., Lopez-Saavedra, A., and Huertas, P. (2014). BRCA1 accelerates CtIP-mediated DNA-end resection. Cell reports *9*, 451-459.

Densham, R.M., Garvin, A.J., Stone, H.R., Strachan, J., Baldock, R.A., Daza-Martin, M., Fletcher, A., Blair-Reid, S., Beesley, J., Johal, B.*, et al.* (2016). Human BRCA1-BARD1 ubiquitin ligase activity counteracts chromatin barriers to DNA resection. Nat Struct Mol Biol *23*, 647-655.

Diaz-Talavera, A., Calvo, P.A., Gonzalez-Acosta, D., Diaz, M., Sastre-Moreno, G., Blanco-Franco, L., Guerra, S., Martinez-Jimenez, M.I., Mendez, J., and Blanco, L. (2019). A cancer-associated point mutation disables the steric gate of human PrimPol. Sci Rep *9*, 1121.

Dong, Z., and Fasullo, M. (2003). Multiple recombination pathways for sister chromatid exchange in Saccharomyces cerevisiae: role of RAD1 and the RAD52 epistasis group genes. Nucleic Acids Res *31*, 2576-2585.

Elvers, I., Johansson, F., Groth, P., Erixon, K., and Helleday, T. (2011). UV stalled replication forks restart by re-priming in human fibroblasts. Nucleic Acids Res *39*, 7049-7057.

Fang, Q. (2013). DNA-protein crosslinks processed by nucleotide excision repair and homologous recombination with base and strand preference in E. coli model system. Mutat Res *741-742*, 1-10.

Fumasoni, M., Zwicky, K., Vanoli, F., Lopes, M., and Branzei, D. (2015). Error-free DNA damage tolerance and sister chromatid proximity during DNA replication rely on the Polalpha/Primase/Ctf4 Complex. Mol Cell *57*, 812-823.

Gallo, D., Kim, T., Szakal, B., Saayman, X., Narula, A., Park, Y., Branzei, D., Zhang, Z., and Brown, G.W. (2019). Rad5 Recruits Error-Prone DNA Polymerases for Mutagenic Repair of ssDNA Gaps on Undamaged Templates. Mol Cell *73*, 900-914 e909.

Garcia-Gomez, S., Reyes, A., Martinez-Jimenez, M.I., Chocron, E.S., Mouron, S., Terrados, G., Powell, C., Salido, E., Mendez, J., Holt, I.J.*, et al.* (2013). PrimPol, an archaic primase/polymerase operating in human cells. Mol Cell *52*, 541-553.

Garcia-Rodriguez, N., Morawska, M., Wong, R.P., Daigaku, Y., and Ulrich, H.D. (2018a). Spatial separation between replisome- and template-induced replication stress signaling. EMBO J *37*.

Garcia-Rodriguez, N., Wong, R.P., and Ulrich, H.D. (2018b). The helicase Pif1 functions in the template switching pathway of DNA damage bypass. Nucleic Acids Res *46*, 8347-8356.

Geacintov, N.E., and Broyde, S. (2017). Repair-Resistant DNA Lesions. Chem Res Toxicol *30*, 1517-1548.

Giannattasio, M., Zwicky, K., Follonier, C., Foiani, M., Lopes, M., and Branzei, D. (2014). Visualization of recombination-mediated damage bypass by template switching. Nat Struct Mol Biol *21*, 884-892.

Guilliam, T.A., and Doherty, A.J. (2017). PrimPol-Prime Time to Reprime. Genes *8*.

Hashimoto, Y., Chaudhuri, A.R., Lopes, M., and Costanzo, V. (2010). Rad51 protects nascent DNA from Mre11-dependent degradation and promotes continuous DNA synthesis. Nat Struct Mol Biol *17*, 1305-1311.

Hoh, L., Gravells, P., Canovas, D., Ul-Hassan, A., Rennie, I.G., Bryant, H., and Sisley, K. (2011). Atypically low spontaneous sister chromatid exchange formation in uveal melanoma. Genes Chromosomes Cancer *50*, 34-42.

IARC (2012). A review of human carcinogens: Chemical agents and related occupations. IARC Monographs on the Evaluation of Carcinogenic Risks to Humans *100F*, 111-144.

Ito, M., Yamamoto, S., Nimura, K., Hiraoka, K., Tamai, K., and Kaneda, Y. (2005). Rad51 siRNA delivered by HVJ envelope vector enhances the anti-cancer effect of cisplatin. J Gene Med *7*, 1044-1052.

Izhar, L., Ziv, O., Cohen, I.S., Geacintov, N.E., and Livneh, Z. (2013). Genomic assay reveals tolerance of DNA damage by both translesion DNA synthesis and homology-dependent repair in mammalian cells. Proc Natl Acad Sci U S A *110*, E1462–E1469.

Johnson, R.D., Liu, N., and Jasin, M. (1999). Mammalian XRCC2 promotes the repair of DNA double-strand breaks by homologous recombination. Nature *401*, 397-399.

Jones, R.M., Kotsantis, P., Stewart, G.S., Groth, P., and Petermann, E. (2014). BRCA2 and RAD51 promote double-strand break formation and cell death in response to gemcitabine. Mol Cancer Ther *13*, 2412-2421.

Kobayashi, K., Guilliam, T.A., Tsuda, M., Yamamoto, J., Bailey, L.J., Iwai, S., Takeda, S., Doherty, A.J., and Hirota, K. (2016). Repriming by PrimPol is critical for DNA replication restart downstream of lesions and chain-terminating nucleosides. Cell Cycle *15*, 1997-2008.

Kolinjivadi, A.M., Sannino, V., De Antoni, A., Zadorozhny, K., Kilkenny, M., Techer, H., Baldi, G., Shen, R., Ciccia, A., Pellegrini, L.*, et al.* (2017). Smarcal1-Mediated Fork Reversal Triggers Mre11-Dependent Degradation of Nascent DNA in the Absence of Brca2 and Stable Rad51 Nucleofilaments. Mol Cell *67*, 867-881.e867.

Kucab, J.E., Zou, X., Morganella, S., Joel, M., Nanda, A.S., Nagy, E., Gomez, C., Degasperi, A., Harris, R., Jackson, S.P.*, et al.* (2019). A Compendium of Mutational Signatures of Environmental Agents. Cell *177*.

Laranjo, L.T., Klaric, J.A., Pearlman, L.R., and Lovett, S.T. (2018). Stimulation of Replication Template-Switching by DNA-Protein Crosslinks. Genes *10*.

Lieberman, R., Xiong, D., James, M., Han, Y., Amos, C.I., Wang, L., and You, M. (2016). Functional characterization of RAD52 as a lung cancer susceptibility gene in the 12p13.33 locus. Mol Carcinog *55*, 953-963.

Livneh, Z., Ziv, O., and Shachar, S. (2010). Multiple two-polymerase mechanisms in mammalian translesion DNA synthesis. Cell Cycle *9*, 729-735.

Lopes, M., Foiani, M., and Sogo, J.M. (2006). Multiple mechanisms control chromosome integrity after replication fork uncoupling and restart at irreparable UV lesions. Mol Cell *21*, 15-27.

Ma, W., Westmoreland, J.W., and Resnick, M.A. (2013). Homologous recombination rescues ssDNA gaps generated by nucleotide excision repair and reduced translesion DNA synthesis in yeast G2 cells. Proc Natl Acad Sci U S A *110*, E2895-2904.

Martinez-Jimenez, M.I., Calvo, P.A., Garcia-Gomez, S., Guerra-Gonzalez, S., and Blanco, L. (2018). The Zn-finger domain of human PrimPol is required to stabilize the initiating nucleotide during DNA priming. Nucleic Acids Res.

Mourón, S., Rodriguez-Acebes, S., Martínez-Jiménez, M.I., García-Gómez, S., Chocrón, S., Blanco, L., and Méndez, J. (2013). Repriming of DNA synthesis at stalled replication forks by human PrimPol. Nat Struct Mol Biol *20*, 1383-1389.

Nakano, T., Morishita, S., Katafuchi, A., Matsubara, M., Horikawa, Y., Terato, H., Salem, A.M., Izumi, S., Pack, S.P., Makino, K., *et al.* (2007). Nucleotide excision repair and homologous recombination systems commit differentially to the repair of DNA-protein crosslinks. Mol Cell *28*, 147-158.

Petermann, E., Orta, M.L., Issaeva, N., Schultz, N., and Helleday, T. (2010). Hydroxyurea-stalled replication forks become progressively inactivated and require two different RAD51-mediated pathways for restart and repair. Mol Cell *37*, 492-502.

Piberger, A.L., Kruger, C.T., Strauch, B.M., Schneider, B., and Hartwig, A. (2018). BPDE-induced genotoxicity: relationship between DNA adducts, mutagenicity in the in vitro PIG-A assay, and the transcriptional response to DNA damage in TK6 cells. Archives of toxicology *92*, 541-551.

Quinet, A., Carvajal-Maldonado, D., Lemacon, D., and Vindigni, A. (2017). DNA Fiber Analysis: Mind the Gap! Methods in enzymology *591*, 55-82.

Rechkoblit, O., Kolbanovskiy, A., Landes, H., Geacintov, N.E., and Aggarwal, A.K. (2017). Mechanism of error-free replication across benzo[a]pyrene stereoisomers by Rev1 DNA polymerase. Nature communications *8*, 965.

Ronson, G.E., Piberger, A.L., Higgs, M.R., Olsen, A.L., Stewart, G.S., McHugh, P.J., Petermann, E., and Lakin, N.D. (2018). PARP1 and PARP2 stabilise

replication forks at base excision repair intermediates through Fbh1-dependent Rad51 regulation. Nature communications *9*, 746.

Rosenbaum, J.C., Bonilla, B., Hengel, S.R., Mertz, T.M., Herken, B.W., Kazemier, H.G., Pressimone, C.A., Ratterman, T.C., MacNary, E., De Magis, A.*, et al.* (2019). The Rad51 paralogs facilitate a novel DNA strand specific damage tolerance pathway. Nature communications *10*, 3515.

Saintigny, Y., Delacote, F., Vares, G., Petitot, F., Lambert, S., Averbeck, D., and Lopez, B.S. (2001). Characterization of homologous recombination induced by replication inhibition in mammalian cells. Embo J *20*, 3861-3870.

Saleh-Gohari, N., Bryant, H.E., Schultz, N., Parker, K.M., Cassel, T.N., and Helleday, T. (2005). Spontaneous homologous recombination is induced by collapsed replication forks that are caused by endogenous DNA single-strand breaks. Mol Cell Biol *25*, 7158-7169.

Schiltz, M., Cui, X.X., Lu, Y.-P., Yagi, H., Jerina, D.M., Zdzienicka, M.Z., Chang, R.L., Conney, A.H., and Wei, S.-J.C. (1999). Characterization of the mutational profile of (+)-7R,8S-dihydroxy-9S,10R-epoxy-7,8,9,10-tetrahydrobenzo[a]pyrene at the hypoxanthine (guanine) phosphoribosyltransferase gene in repair-deficient Chinese hamster V-H1 cells. Carcinogenesis *20*, 2279-2286.

Schlacher, K., Christ, N., Siaud, N., Egashira, A., Wu, H., and Jasin, M. (2011). Double-Strand Break Repair-Independent Role for BRCA2 in Blocking Stalled Replication Fork Degradation by MRE11. Cell *145*, 529-542.

Schneider, C.A., Rasband, W.S., and Eliceiri, K.W. (2012). NIH Image to ImageJ: 25 years of image analysis. Nat Methods *9*, 671-675.

Svikovic, S., Crisp, A., Tan-Wong, S.M., Guilliam, T.A., Doherty, A.J., Proudfoot, N.J., Guilbaud, G., and Sale, J.E. (2018). R-loop formation during S phase is restricted by PrimPol-mediated repriming. Embo j.

Vallerga, M.B., Mansilla, S.F., Federico, M.B., Bertolin, A.P., and Gottifredi, V. (2015). Rad51 recombinase prevents Mre11 nuclease-dependent degradation and excessive PrimPol-mediated elongation of nascent DNA after UV irradiation. Proc Natl Acad Sci U S A *112*, E6624-6633.

Villalta, P.W., Hochalter, J.B., and Hecht, S.S. (2017). Ultrasensitive High-Resolution Mass Spectrometric Analysis of a DNA Adduct of the Carcinogen Benzo[a]pyrene in Human Lung. Analytical chemistry *89*, 12735-12742.

Wang, Y., McKay, J.D., Rafnar, T., Wang, Z., Timofeeva, M.N., Broderick, P., Zong, X., Laplana, M., Wei, Y., Han, Y.*, et al.* (2014). Rare variants of large effect in BRCA2 and CHEK2 affect risk of lung cancer. Nat Genet *46*, 736-741.

Zamborszky, J., Szikriszt, B., Gervai, J.Z., Pipek, O., Poti, A., Krzystanek, M., Ribli, D., Szalai-Gindl, J.M., Csabai, I., Szallasi, Z.*, et al.* (2017). Loss of BRCA1 or BRCA2 markedly increases the rate of base substitution mutagenesis and has distinct effects on genomic deletions. Oncogene *36*, 746-755.

Zellweger, R., Dalcher, D., Mutreja, K., Berti, M., Schmid, J.A., Herrador, R., Vindigni, A., and Lopes, M. (2015). Rad51-mediated replication fork reversal is a global response to genotoxic treatments in human cells. J Cell Biol *208*, 563-579.

Zhou, Y., Caron, P., Legube, G., and Paull, T.T. (2014). Quantitation of DNA double-strand break resection intermediates in human cells. Nucleic Acids Res *42*, e19.

Acknowledgements

We thank Siobhan Murphy-Hollies for help with qRT-PCR, Prof Juan Mendez for his kind gift of PrimPol expression constructs, and Drs Rebecca M. Jones, Katarzyna Starowicz and Karen Sisley for advice on PFGE and SCE quantification. This work was supported by the German Research Foundation (PI 1300/1-1), Cancer Research UK Birmingham Centre Development Fund, Medical Research Council (MR/S021310/1), University of Sheffield (322149), Wellcome Trust (206343/Z/17/Z) and Cancer Research UK (C8820/A19062).

Author contributions

A.L.P. conceived the study; A.L.P., A.K.W. and H.E.B. performed the experiments; A.L.P., A.K.W., J.R.M., H.E.B. and E.P. designed the experiments; A.L.P. and E.P. and wrote the paper.

Declaration of Interests

The authors declare that they have no competing financial interest.

Figure Legends

Figure 1. Bulky DNA adducts induce RAD51 foci without replication fork stalling or -collapse

(A) Schematic of DNA repair and damage tolerance pathways induced by low doses of BPDE, which forms bulky adducts on guanine. NER: nucleotide excision repair; TLS: translesion synthesis; HR: homologous recombination.

(B) Co-localisation of γH2AX and replication forks in U2OS cells after 1 h release from 1650 nM BPDE treatment for 20 min. DNA was denatured with HCl to allow CldU detection. Cells were immunostained for CldU (red) and γH2AX (green). Scale bars are 10 µm.
(C) Percentages of U2OS cells with > 8 γH2AX foci after release from increasing concentrations of BPDE for the times indicated. n=3
(D) Representative images of BPDE-induced RAD51 foci.
(E) Percentages of U2OS cells with > 5 RAD51 foci after release from increasing concentrations of BPDE for the times indicated. n = 3-5
(F) Percentages of stalled forks after release from BPDE. U2OS cells were pulse labelled with CldU, treated with BPDE during the CldU pulse, and released into IdU. n=4 (1650 nM n=3).
(G) Percentages of cells with > 10 53BP1 foci after release from increasing concentrations of BPDE for the times indicated. n=3-4
(H) Top: Protein levels of RAD51 and α-Tubulin (loading control) in U2OS cells after 48 h depletion with RAD51 or non-targeting (nonT) siRNA. Bottom: Strategy for DNA fibre labelling.
(I) Percentages of stalled forks after release from 50 nM BPDE as shown in (H) in cells treated with nonT or RAD51 siRNA for 48 h. n=3
(J) Percentages of control- or RAD51-depleted U2OS cells with > 10 53BP1 foci after release from 50 nM BPDE. n=3
The means and SEM (bars) of at least three independent experiments are shown. Asterisks indicate p-values compared to control unless indicated otherwise (student's t-test, * $p < 0.05$, ** $p < 0.01$, *** $p < 0.001$).

Figure 2. RAD51 is required for resolution of single-stranded DNA gaps that form at bulky adducts via PrimPol-dependent re-priming
(A) Percentages of control- or RAD51-depleted U2OS cells with > 10 RPA foci after release from BPDE for the times indicated. n=3
(B) Schematic of the S1 endonuclease-modified DNA fibre assay and strategy for DNA fibre labelling.
(C) CldU/IdU ratios after S1-modified DNA fibre assay in cells treated with solvent or 50 nM BPDE as in (B).

(D) Schematic of RAD51-mediated ssDNA gap repair after re-priming at replication-blocking lesions.
(E) *PRIMPOL* mRNA quantification by qRT-PCR after 48 h siRNA transfection. *PRIMPOL* mRNA levels were normalised to *RPLP0* and control. n=3
(F) Quantification of stalled forks after release from 50 nM BPDE in presence of non-targeting (nonT) or PrimPol siRNA. Fibre labelling was according to Fig. 1H. n=3-4
(G) CldU/IdU ratios after S1-modified DNA fibre assay in cells treated with solvent or 50 nM BPDE as in (B) after 48 h of control or PrimPol siRNA.
(H) Protein domain structure of wild type (WT) and primase-dead (CH) PrimPol variants. The CH variant has two point mutations (CH > GY) in the zinc finger (ZnF) domain.
(I) Protein levels of V5-tagged WT or CH PrimPol after co-transfection of cells with nonT or PrimPol siRNA and expression constructs encoding WT or CH PrimPol for 48 h.
(J) Quantification of stalled forks after release from 50 nM BPDE in presence of nonT (-) or PrimPol siRNA and expression constructs encoding GFP (-) or WT or CH PrimPol. n=3
The means and SEM (bars) of at least three independent experiments are shown. Asterisks indicate p-values compared to control unless indicated otherwise (student's t-test, * $p < 0.05$, ** $p < 0.01$, *** $p < 0.001$).

Figure 3. PrimPol-mediated re-priming and further end processing promote RAD51 loading at bulky DNA adducts.
(A) Representative images of RAD51 foci after 24 h release from 50 nM BPDE in presence of nonT or PrimPol siRNA. Scale bars are 10 µm.
(B) Percentages of cells with >5 RAD51 foci after release from 50 nM BPDE for the times indicated, in presence of nonT or PrimPol siRNA. n=3
(C) Percentages of cells with >5 RAD51 foci after release from 50 nM BPDE for the times indicated, in presence of nonT (-) or PrimPol siRNA and expression constructs encoding GFP or WT or CH PrimPol. n=3

(D) Schematic representation of MRE11's nuclease activities and respective chemical inhibitors PFM01 and mirin.
(E) Strategy for SMART analysis of single-stranded DNA quantifications and representative pictures of native DNA tracts. Scale bars are 5 µm.
(F) SMART analysis of single-stranded DNA after release from 20 min of 50 nM BPDE for 4 h, in presence or absence of MRE11 inhibitor PFM01.
(G) Percentages of cells with >5 RAD51 foci after release from 50 nM BPDE for the times indicated, in presence or absence of MRE11 inhibitors mirin or PFM01. Treatment was as shown in (E). n=3
(H) Percentages of cells with >5 RAD51 foci after release from 50 nM BPDE for the times indicated, in presence of nonT or EXO1 siRNA for 48 h. Inset: Protein levels of EXO1 and α-Tubulin (loading control) in U2OS cells after 48 h depletion with EXO1 or nonT siRNA. n=3-4
The means and SEM (bars) of at least three independent experiments are shown. Asterisks indicate p-values (student's t-test, * $p < 0.05$, ** $p < 0.01$, *** $p < 0.001$). n=4

Figure 4. PrimPol promotes RAD51 loading at bulky adducts more generally, but not in response to DSB-inducing conditions.
(A) Strategy for the S1-modified DNA fibre assay with UV irradiation.
(B) CldU/IdU ratios after S1-modified DNA fibre assay in cells treated with 5 J/m^2 UV or mock-treated as in (A), in presence of nonT or PrimPol siRNA.
(C) Percentages of cells with >5 RAD51 foci after release from 5 J/m^2 UV for the times indicated, in presence of nonT or PrimPol siRNA. n=3
(D) Percentages of cells with >5 RAD51 foci after release from 500 nM BPDE for the times indicated, in presence of nonT or PrimPol siRNA. n=3
(E) Percentages of cells with >5 RAD51 foci after treatment with 2 mM HU for 24 h, in presence of nonT or PrimPol siRNA. n=3
(F) Percentages of EdU positive cells with >10 RAD51 foci after release from 2 Gy IR for the time indicated, in presence of nonT or PrimPol siRNA. n=3
The means and SEM (bars) of at least three independent experiments are shown. Asterisks indicate p-values (student's t-test, * $p < 0.05$, ** $p < 0.01$, *** $p < 0.001$).

Figure 5. PrimPol is required for homologous recombination induced by bulky adducts.

(A) Relative recombination frequencies in SW480SN.3 cells induced by BPDE. Cells were treated with 50 nM BPDE for 20 min. n=4 (nonT solvent n=3)

(B) Colony survival assay of U2OS cells after 20 min treatment with BPDE at the indicated concentrations in presence of nonT, PrimPol or RAD51 siRNA. n=4 (RAD51 siRNA n=3)

(C) Strategy for detection of SCEs and representative picture of metaphase spreads in response to 50 nM BPDE.

(D) SCE formation in U2OS cells after treatment with 50 nM BPDE or solvent for 20 min and release for 48 h. n=3

(E) SCE formation in U2OS cells after treatment with 50 nM BPDE or solvent in presence of nonT or PrimPol siRNA. n=3

(F) Model of recombination at bulky DNA adducts. Left: In presence of PrimPol, re-priming creates gaps that are resected for RAD51 foci formation and recombination repair. Right: In absence of PrimPol, bulky DNA adducts are either bypassed by TLS or alternatively, stalled forks are stabilised by fork regression and potential rescue upon convergence with another fork.

The means and SEM (bars) of at least three independent experiments are shown. Asterisks indicate p-values (student's t-test, * $p < 0.05$, ** $p < 0.01$, *** $p < 0.001$).

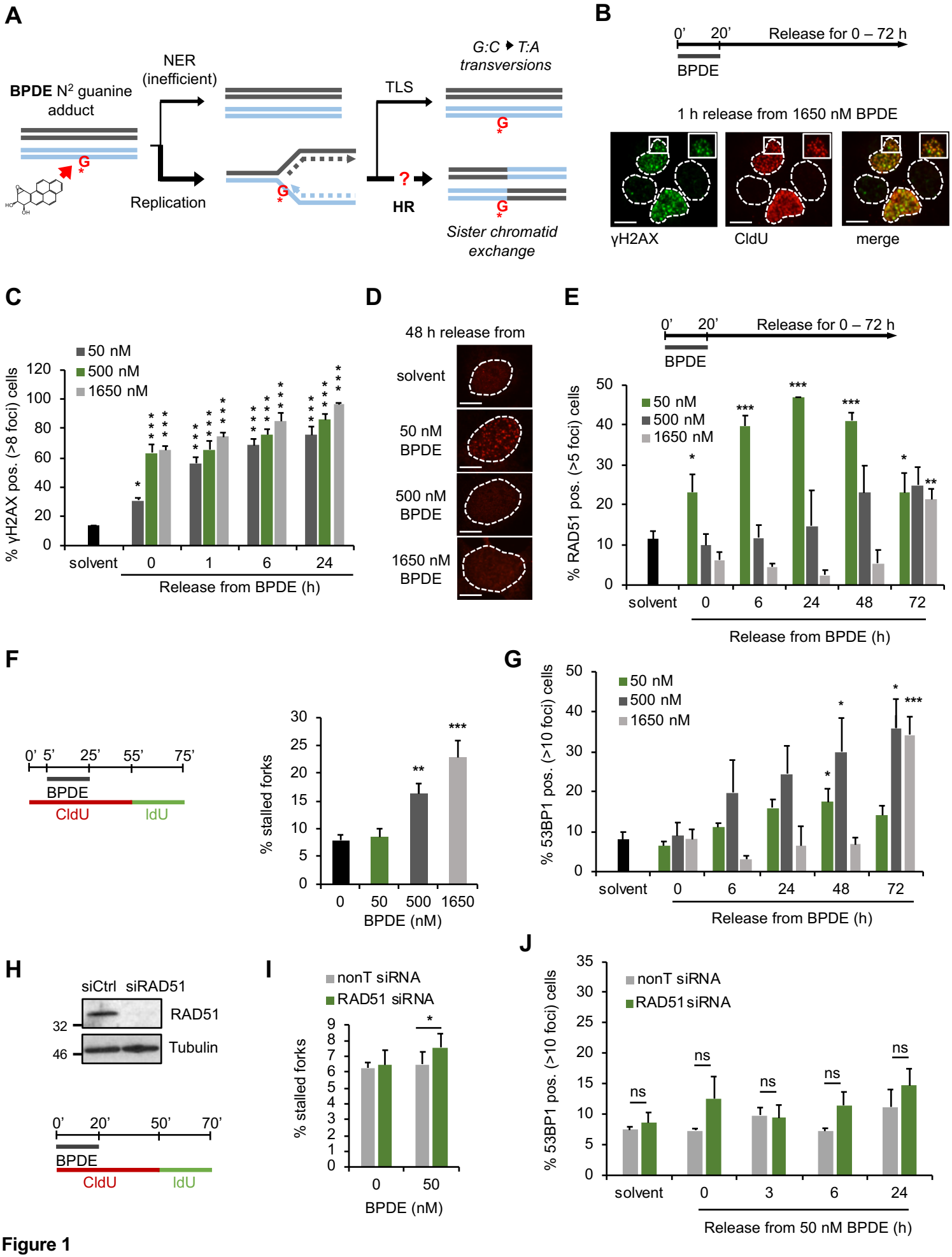
A
BPDE N2 guanine adduct
NER (inefficient)
Replication
TLS
G:C ▶ T:A transversions
HR
Sister chromatid exchange
B
0'
20'
Release for 0 – 72 h
BPDE
1 h release from 1650 nM BPDE
γH2AX
CldU
merge
C
50 nM
500 nM
1650 nM
% γH2AX pos. (>8 foci) cells
solvent
Release from BPDE (h)
D
48 h release from
solvent
50 nM BPDE
500 nM BPDE
1650 nM BPDE
E
% RAD51 pos. (>5 foci) cells
F
0' 5' 25' 55' 75'
BPDE
CldU
IdU
% stalled forks
BPDE (nM)
G
% 53BP1 pos. (>10 foci) cells
H
siCtrl siRAD51
RAD51
Tubulin
32
46
0' 20' 50' 70'
I
nonT siRNA
RAD51 siRNA
J
ns
Release from 50 nM BPDE (h)

Figure 1

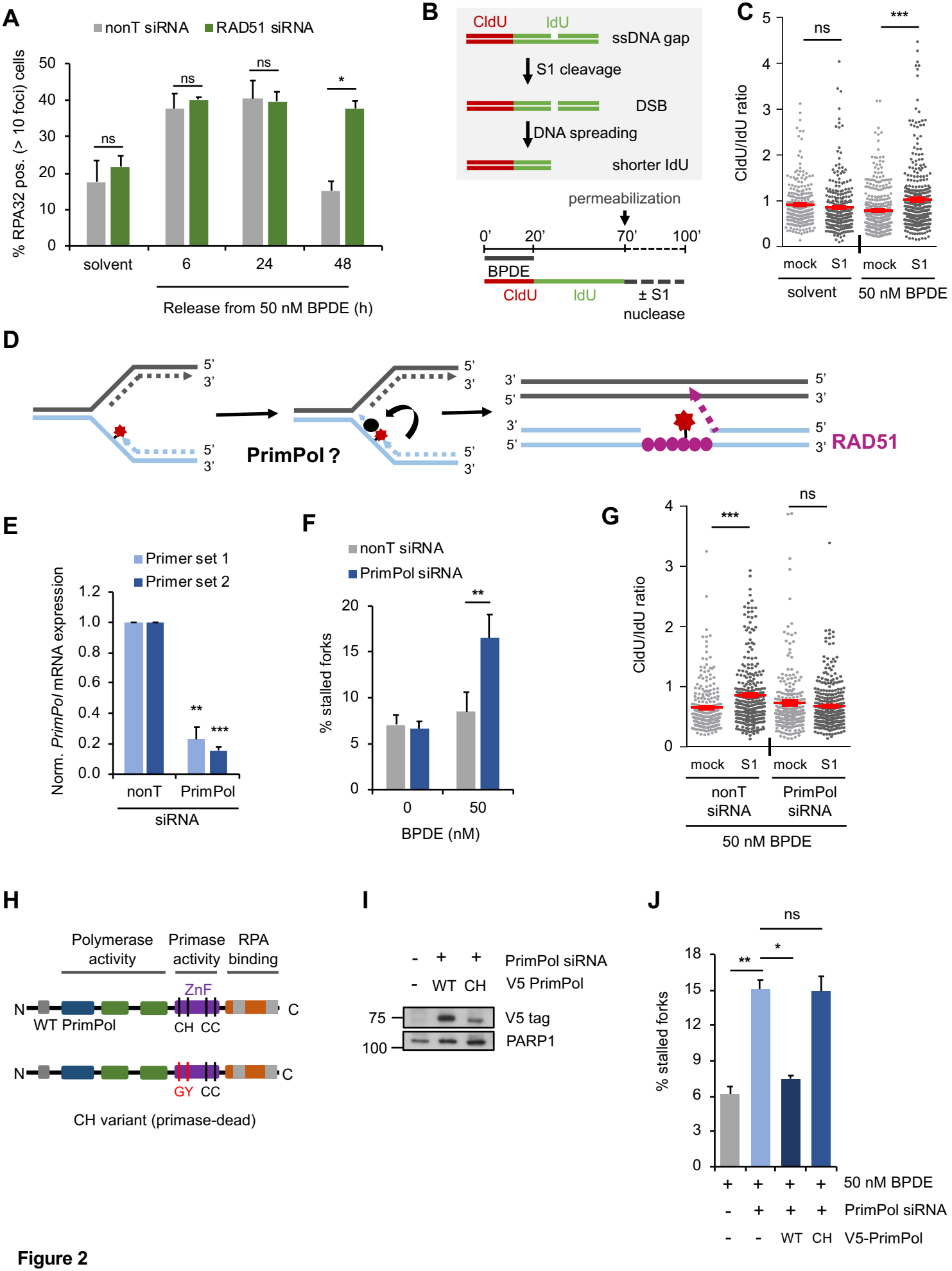
A
nonT siRNA
RAD51 siRNA
% RPA32 pos. (> 10 foci) cells
ns
ns
ns
*
solvent
6
24
48
Release from 50 nM BPDE (h)
B
CldU
IdU
ssDNA gap
S1 cleavage
DSB
DNA spreading
shorter IdU
permeabilization
0'
20'
70'
100'
BPDE
CldU
IdU
± S1 nuclease
C
CldU/IdU ratio
ns
***
mock
S1
mock
S1
solvent
50 nM BPDE
D
5'
3'
PrimPol ?
RAD51
E
Primer set 1
Primer set 2
Norm. PrimPol mRNA expression
**
***
nonT
PrimPol
siRNA
F
nonT siRNA
PrimPol siRNA
% stalled forks
**
0
50
BPDE (nM)
G
CldU/IdU ratio
***
ns
mock
S1
mock
S1
nonT siRNA
PrimPol siRNA
50 nM BPDE
H
Polymerase activity
Primase activity
RPA binding
ZnF
N
C
WT PrimPol
CH CC
GY CC
CH variant (primase-dead)
I
PrimPol siRNA
V5 PrimPol
WT
CH
75
100
V5 tag
PARP1
J
ns
*
**
% stalled forks
50 nM BPDE
PrimPol siRNA
V5-PrimPol
WT
CH

Figure 2

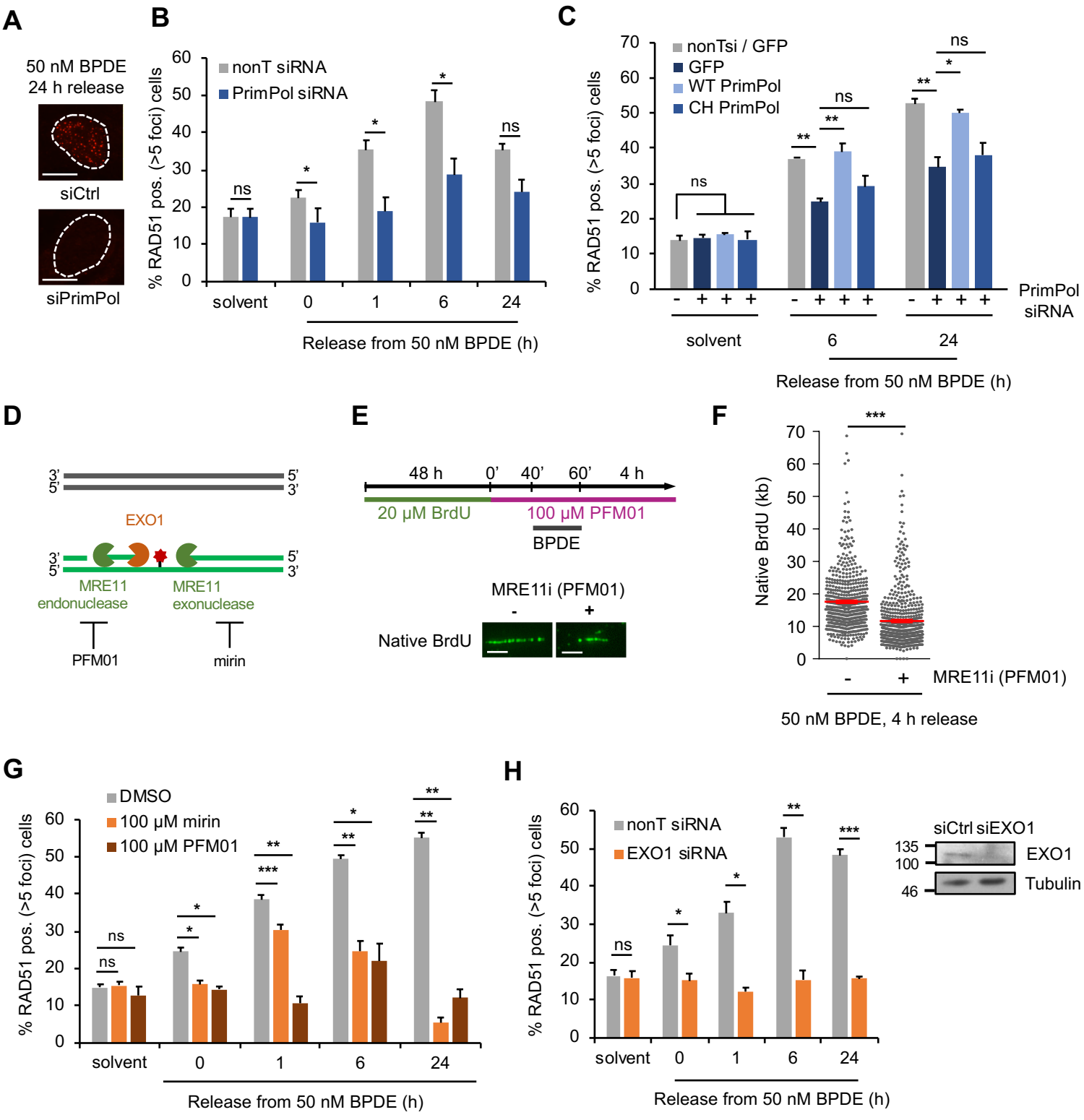
A
50 nM BPDE
24 h release
siCtrl
siPrimPol
B
nonT siRNA
PrimPol siRNA
% RAD51 pos. (>5 foci) cells
solvent
0
1
6
24
Release from 50 nM BPDE (h)
C
nonTsi / GFP
GFP
WT PrimPol
CH PrimPol
% RAD51 pos. (>5 foci) cells
PrimPol siRNA
solvent
6
24
Release from 50 nM BPDE (h)
D
EXO1
MRE11 endonuclease
MRE11 exonuclease
PFM01
mirin
E
48 h
0'
40'
60'
4 h
20 μM BrdU
100 μM PFM01
BPDE
MRE11i (PFM01)
Native BrdU
F
Native BrdU (kb)
MRE11i (PFM01)
50 nM BPDE, 4 h release
G
DMSO
100 μM mirin
100 μM PFM01
% RAD51 pos. (>5 foci) cells
solvent
Release from 50 nM BPDE (h)
H
nonT siRNA
EXO1 siRNA
% RAD51 pos. (>5 foci) cells
siCtrl siEXO1
EXO1
Tubulin
Release from 50 nM BPDE (h)

Figure 3

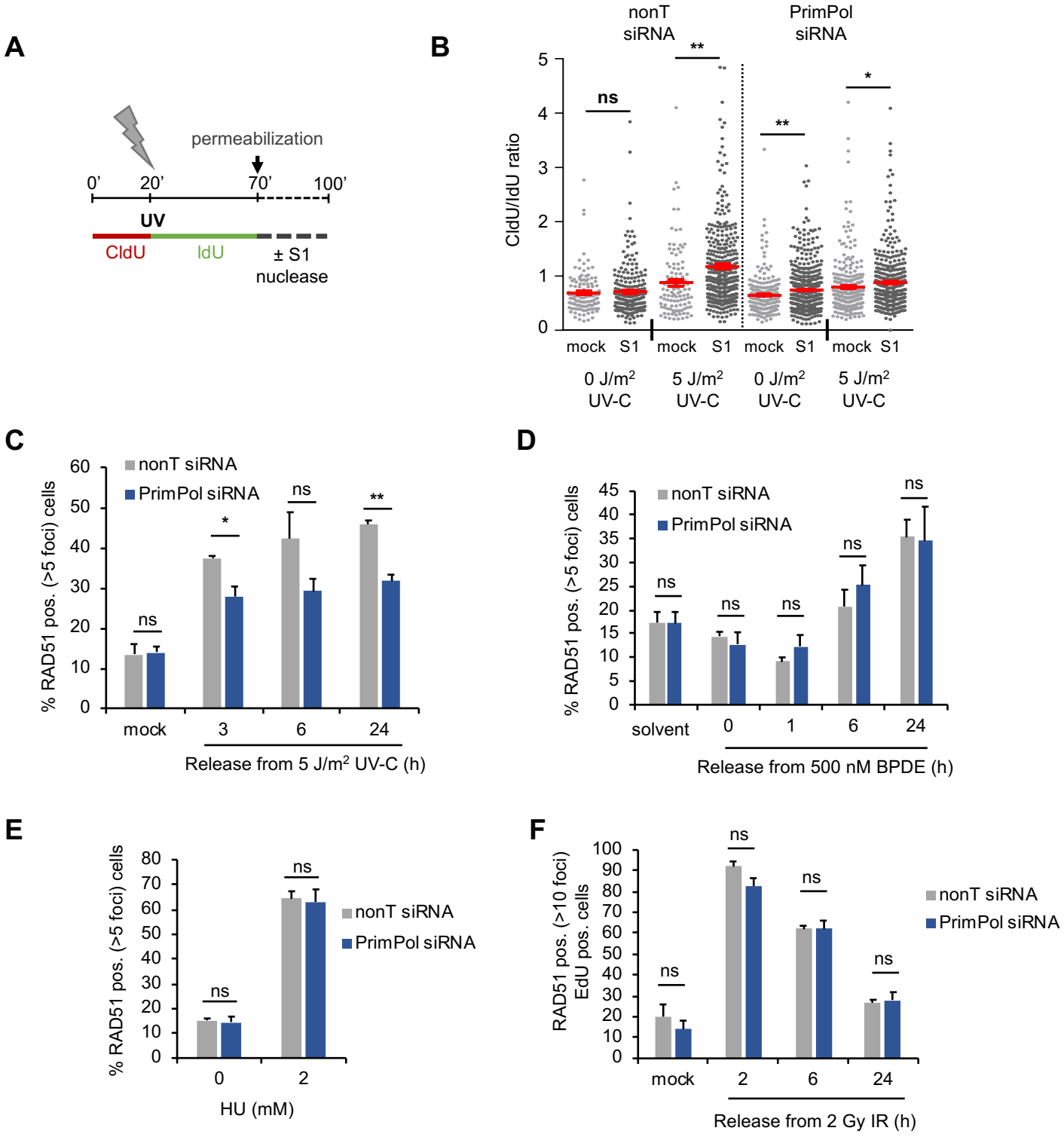
A
permeabilization
0'
20'
70'
100'
UV
CldU
IdU
± S1
nuclease
B
nonT
siRNA
PrimPol
siRNA
CldU/IdU ratio
ns
**
**
*
mock
S1
0 J/m2
UV-C
5 J/m2
UV-C
C
nonT siRNA
PrimPol siRNA
% RAD51 pos. (>5 foci) cells
Release from 5 J/m2 UV-C (h)
D
nonT siRNA
PrimPol siRNA
% RAD51 pos. (>5 foci) cells
solvent
Release from 500 nM BPDE (h)
E
% RAD51 pos. (>5 foci) cells
nonT siRNA
PrimPol siRNA
HU (mM)
F
RAD51 pos. (>10 foci)
EdU pos. cells
nonT siRNA
PrimPol siRNA
Release from 2 Gy IR (h)

Figure 4

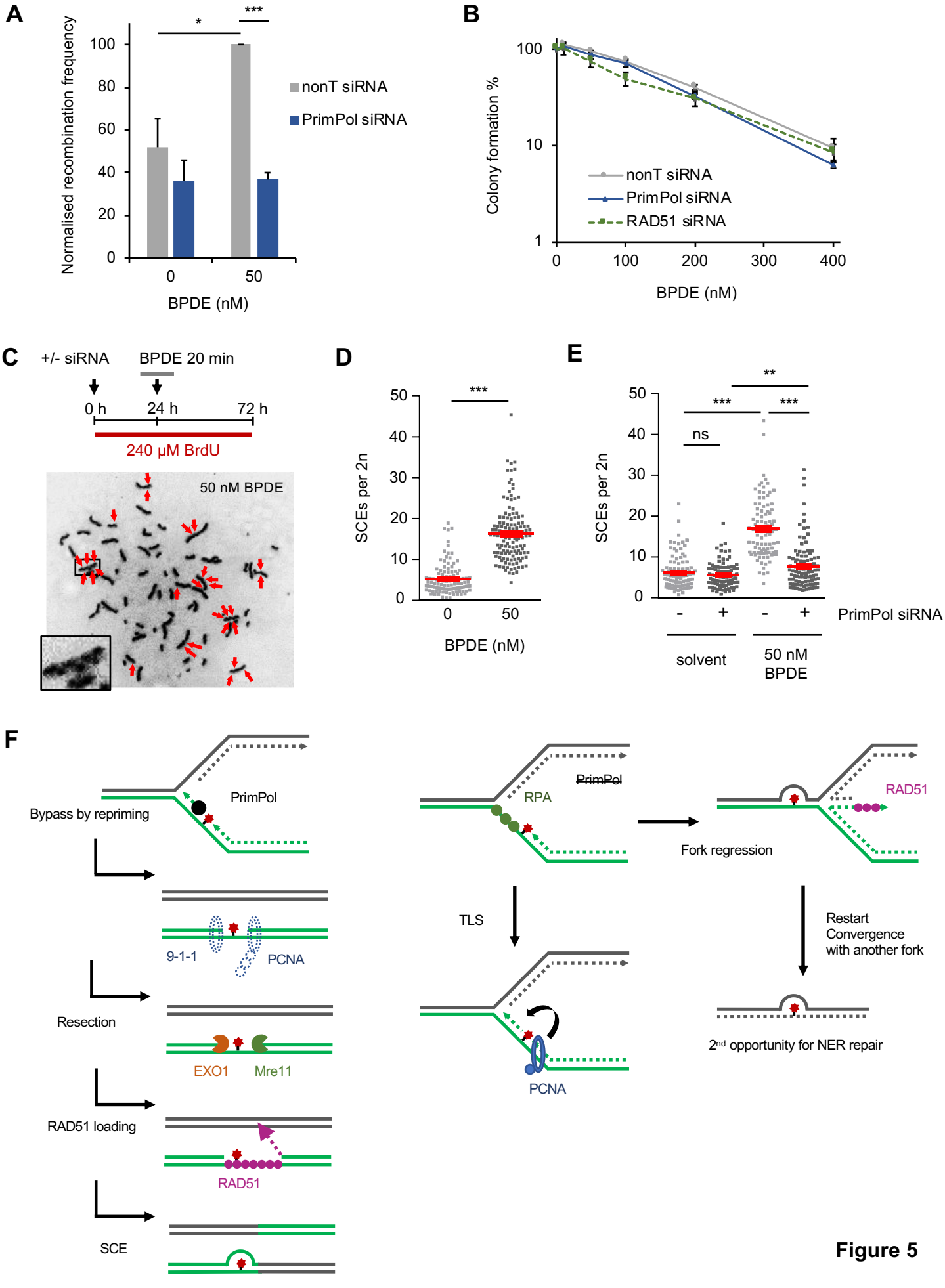
A
Normalised recombination frequency
100
80
60
40
20
0
*
***
nonT siRNA
PrimPol siRNA
0
50
BPDE (nM)
B
Colony formation %
100
10
1
nonT siRNA
PrimPol siRNA
RAD51 siRNA
0
100
200
300
400
BPDE (nM)
C
+/- siRNA
BPDE 20 min
0 h
24 h
72 h
240 μM BrdU
50 nM BPDE
D
SCEs per 2n
50
40
30
20
10
0
***
0
50
BPDE (nM)
E
SCEs per 2n
**
***
***
ns
PrimPol siRNA
-
+
-
+
solvent
50 nM BPDE
F
Bypass by repriming
PrimPol
9-1-1
PCNA
Resection
EXO1
Mre11
RAD51 loading
RAD51
SCE
PrimPol
RPA
Fork regression
RAD51
TLS
Restart Convergence with another fork
PCNA
2nd opportunity for NER repair

Figure 5

Supplemental Information

PrimPol-dependent single-stranded gap formation mediates homologous recombination at bulky DNA adducts

Ann Liza Piberger, Alexandra K Walker, Joanna R Morris, Helen E Bryant, Eva Petermann

Supplemental Figures

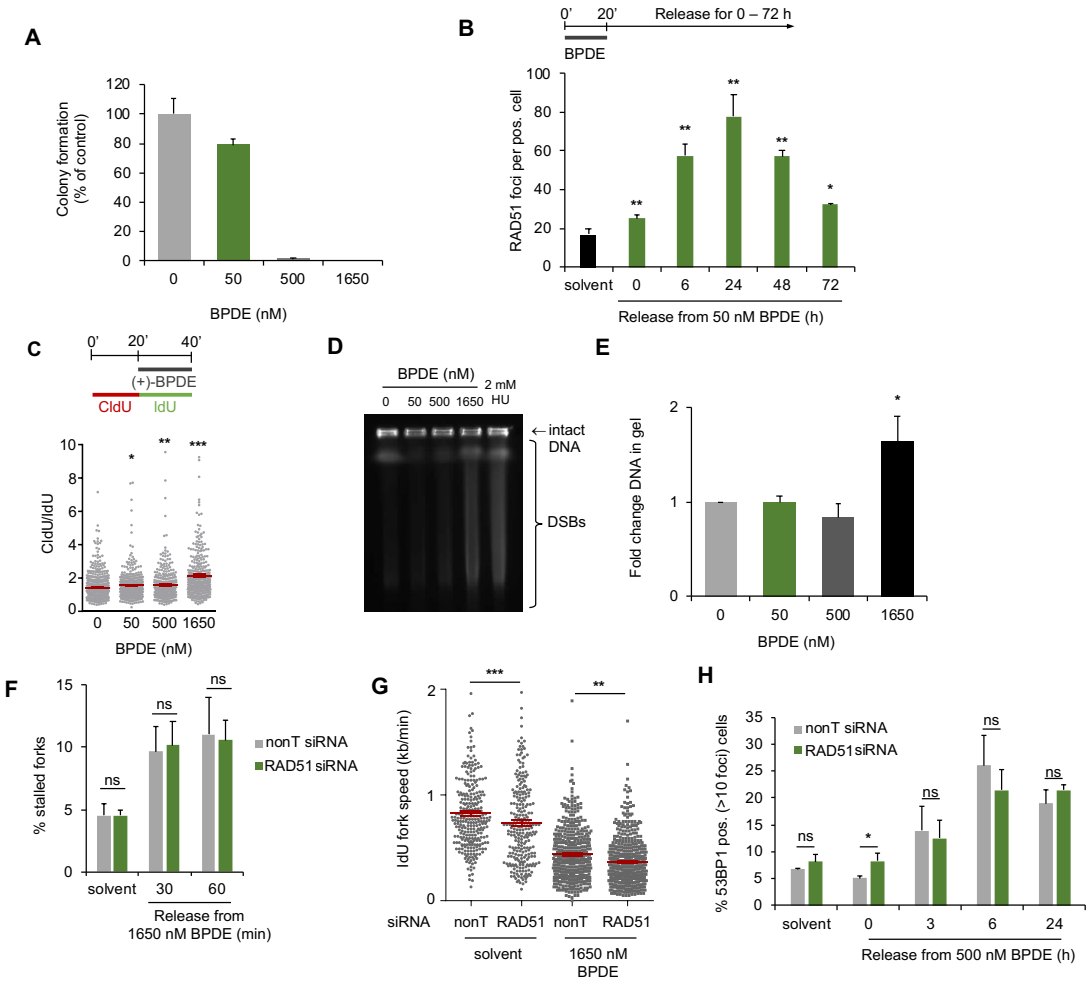

Fig S1. Replication stress and HR induced by different BPDE concentrations. (A) Colony survival of U2OS cells after release from 20 min BPDE at the indicated concentrations. n=1 (B) Numbers of RAD51 foci per RAD51 foci positive cell after release from 50 nM BPDE for the times indicated. n=3 (C) CldU/IdU ratios after DNA fibre assay with the indicated concentrations of BPDE present during the IdU pulse. Increased CldU/IdU ratios indicate BPDE-induced fork slowing. (D) Pulse-field gel electrophoresis (PFGE) to visualise DSBs in after 3 hours release from increasing concentrations of BPDE. Treatment with 2 mM HU for 48 hours was included as a positive control. (E) Quantification of PFGE. n= 5 (F) Quantification of stalled forks after release from 1650 nM BPDE for 30 or 60 min in cells treated with nonT or RAD51 siRNA. n=3 (G) Replication fork speeds in cells 30 min released from treatment with 1650 nM BPDE in presence or absence of RAD51 siRNA. (H) Percentages of control- or RAD51-depleted U2OS cells with > 10 53BP1 foci after release from 500 nM BPDE. n=3. The means and SEM (bars) of independent experiments are shown. Asterisks indicate p-values compared to control unless indicated otherwise (student's t-test, * $p < 0.05$, ** $p < 0.01$, *** $p < 0.001$).

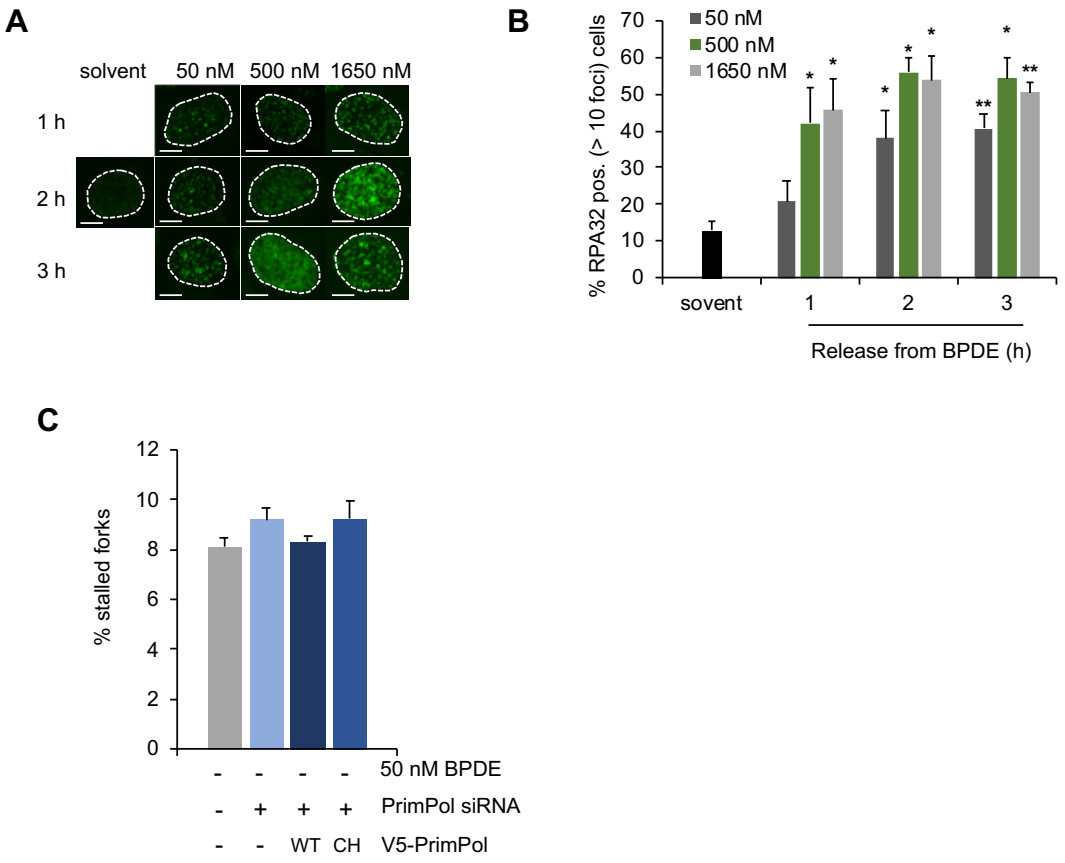

Fig S2. BPDE induces single-stranded DNA gaps. (A) Representative images of RPA foci after release from 20 min BPDE as indicated. (B) Percentages of U2OS cells with > 10 RPA foci after release from BPDE for the times indicated. n=3 (C) Quantification of stalled forks after release from solvent in presence or absence of nonT (-) or PrimPol siRNA and expression constructs encoding GFP (-) or WT or CH PrimPol. n=2**.** The means and SEM (bars) of independent experiments are shown. Asterisks indicate p-values compared to control (student's t-test, * $p < 0.05$, ** $p < 0.01$, *** $p < 0.001$).

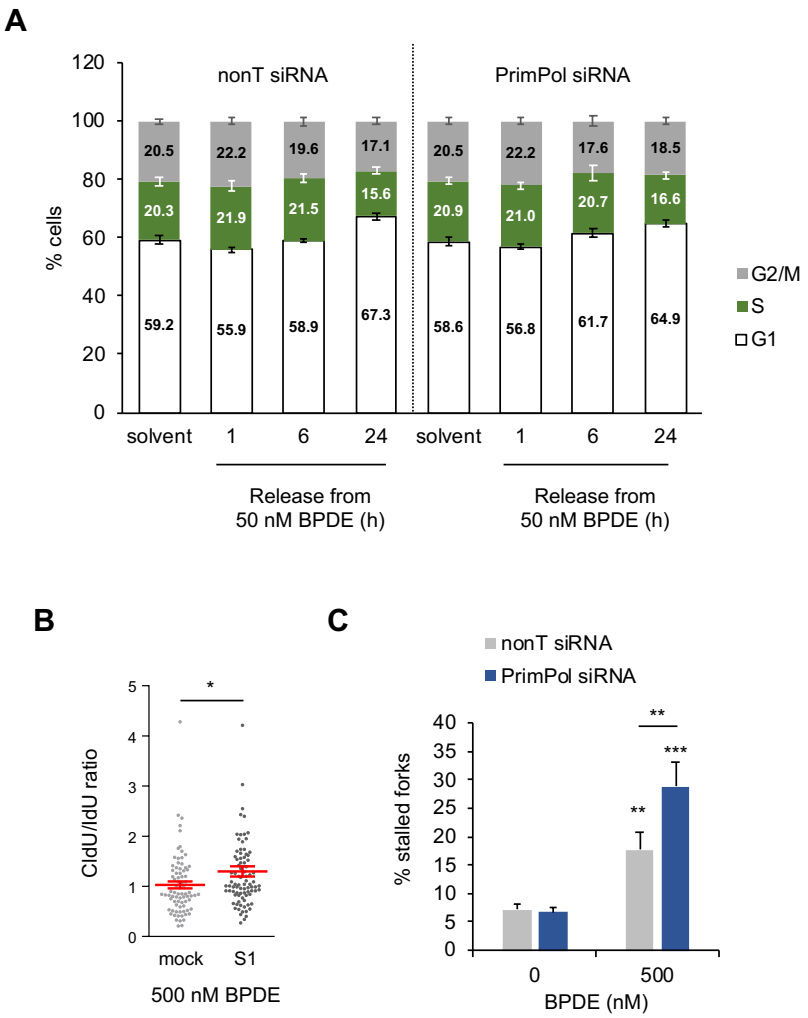

Fig. S3. PrimPol depletion does not alter cell cycle distribution. (A) FACS analysis of cell cycle distributions after release from solvent or 50 nM BPDE in presence of nonT or PrimPol siRNA. Release from solvent was for 1 hour. n=3-4. (B) CldU/IdU ratios after S1-modified DNA fibre assay in cells treated with 500 nM BPDE as in Fig. 2B. (C) Quantification of stalled forks after release from 500 nM BPDE in presence of non-targeting (nonT) or PrimPol siRNA. Fibre labelling was according to Fig. 1H. n=3. The means and SEM (bars) of independent experiments are shown. Asterisks indicate p-values (student's t-test, * $p < 0.05$, ** $p < 0.01$, *** $p < 0.001$).

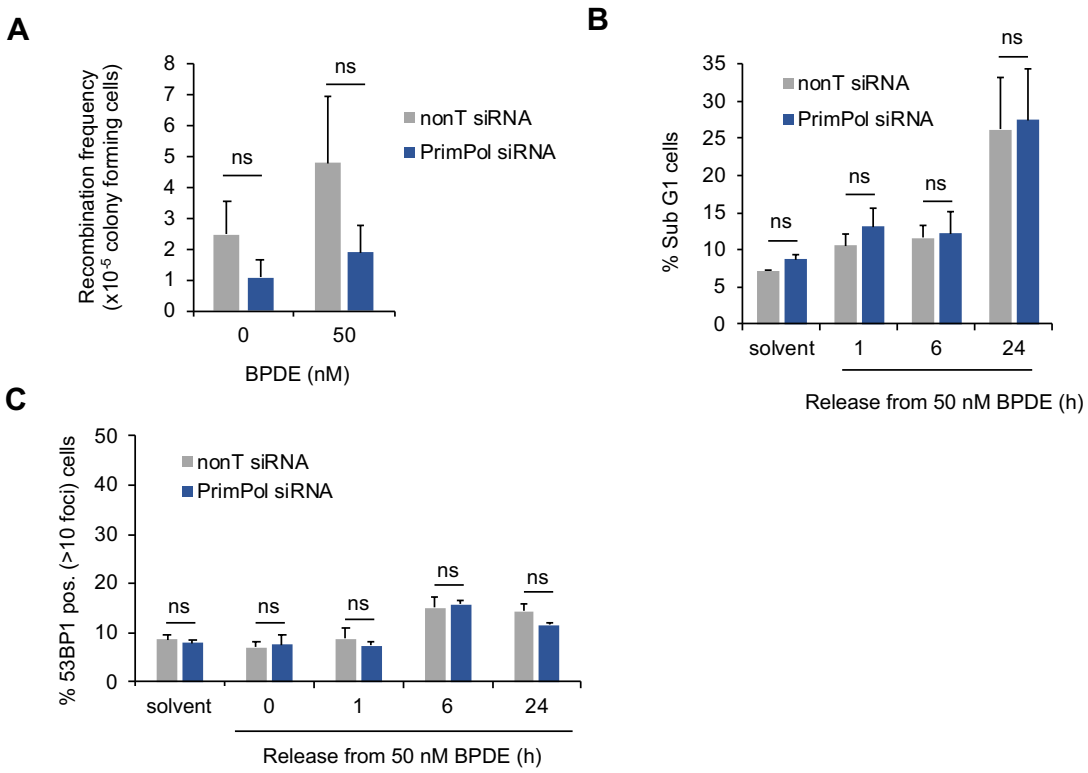

Fig. S4. Impact of PrimPol on recombination, cell death and DSB formation induced by bulky adducts. (A) Absolute recombination frequencies in SW480SN.3 cells induced by 50 nM BPDE presence of nonT or PrimPol siRNA. n=3-4 (B) FACS analysis of percentages of sub-G1 cells after release from solvent or 50 nM BPDE in presence of nonT or PrimPol siRNA. Release from solvent was for 1 hour. n=3-4 (C) Percentages of control- or PrimPol-depleted U2OS cells with > 10 53BP1 foci after release from 50 nM BPDE. n=3**.** The means and SEM (bars) of independent experiments are shown.

Supplementary Table S1. Sequences of PCR primers

Name	Sequence (5' → 3')
PRIMPOL1 For	CCGAGGTATCCCAGAGGTGA
PRIMPOL1 Rev	AATGCCCCACGTTGCTTTTC
PRIMPOL2 For	AAAAGCAACGTGGGGCATTC
PRIMPOL2 Rev	GGTGGTTCTTCTGGCTTGGA
RPLP0 For (control)	CAGATTGGCTACCCAACTGTT
RPLP0 Rev (control)	GGAAGGTGTAATCCGTCTCCAC